CHEMISTRY OF MATERIALS

Article

pubs.acs.org/cm

Nanoscale Dispersions of Gelled SnO_2: Material Properties and Device Applications

Brion Bob, Tze-Bin Song, Chun-Chao Chen, Zheng Xu, and Yang Yang*

Department of Materials Science and Engineering and California NanoSystems Institute, University of California at Los Angeles, Los Angeles, California 90025, United States

ABSTRACT: High intrinsic carrier mobility and excellent transparency at visible wavelengths make stannic oxide (SnO_2) a material of interest for a variety of optoelectronic applications. Here, we demonstrate a solvothermal route to stabilize gelled dispersions of tin oxide nanoparticles with diameters in the range of 2−4 nm. Small particle dimensions ultimately allow for the deposition of smooth thin films with all of the useful properties that can be expected from this material system. The structural and morphological properties of the deposited films are investigated, and they are demonstrated as an electron collection layer in polymer-based organic photovoltaic cells with promising power conversion efficiencies.

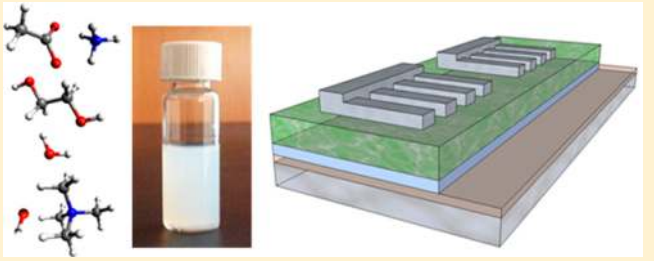

KEYWORDS: *tin oxide, sol−gel, nanoparticles, solar cells, OPV*

INTRODUCTION

Tin(IV) oxide (SnO_2) is a wide-bandgap metal oxide that has become ubiquitous in the development of thin film transistors,[1−3] solar cells,[4−7] batteries,[8−10] and a variety of other optical and electronic devices.[11−14] The high mobility value of bulk SnO_2, compared to other *n*-type oxides, offers advantages in nearly any application that requires efficient carrier transport. This particular property has been emphasized recently by the remarkably high mobility values reported in solution-processed tin oxide thin film transistors.[15] The success of doped tin oxide at favorably inducing current collection in dye-sensitized,[16,17] amorphous silicon,[18] and metal chalcogenide[19,20] solar cells has made it a common feature in the majority of high efficiency devices and fabrication recipes.

The multivalent chemistry of tin species in solution allows for the facile formation of extended gel structures when appropriate tin precursors are hydrolyzed in solution. The rapid formation of metal oxide bonds then grows rapidly, eventually consuming all of the available precursor species. Ensuring that the growing gel particles maintain nanoscale dimensions generally requires some form of surfactant, ligand, or capping agent to be present in the growth solution. The presence of anions such as chloride and acetate can provide some degree of shape control for the growing particles, and are most commonly used when a hydrothermal treatment can be applied after precipitation in order to decompose the resulting gelled bond structures into dense crystallites. The resulting particles tend to show a wide range of dimensions from several tens to hundreds of nanometers, depending on the details of the recipe.

The high temperatures (180−250 °C) typically used for hydrothermal processing create an increased tendency toward the formation of large particles during synthesis,[21] but are often necessary to ensure the crystallinity of the reaction products. The use of neutral pH values, rather than those created by inherently acidic tin precursors, has also been identified as a potential to improve the crystallization of the resulting nanoscale and microscale product.[22] Guided by each of these observations, we have constructed a solvothermal reaction route that makes use of moderate reaction temperatures (120−170 °C) to form dispersions of SnO_2 nanoparticles without the need for pressurized reaction vessels. However, synthesis reactions that employ this method subject themselves to significant risk of particle agglomeration and precipitation unless appropriate measures are taken to separate the growing crystallites.

We have found that tetraalkylammonium ions serve as effective ligands to separate and define the morphology of extremely small gelled tin oxide nanoparticles 2−4 nm in diameter. The resulting nanoparticles are easily dispersed in polar solvents, and assemble into compact thin films upon deposition and drying. The existence of metal-oxide bonding in the nanoparticle inks prior to deposition allows for their use in semiconductor devices without extensive annealing in air, making them potentially useful for applications involving thermally sensitive or easily oxidized materials and substrates. Efficient organic photovoltaic devices have been fabricated using films of the gelled tin oxide nanoparticles as the electron transport layer in order to demonstrate the compatibility of this material with existing solution processed organic semiconductors.

Received: July 22, 2013
Revised: November 8, 2013

   dx.doi.org/10.1021/cm402462m | *Chem. Mater.* XXXX, XXX, XXX−XXX

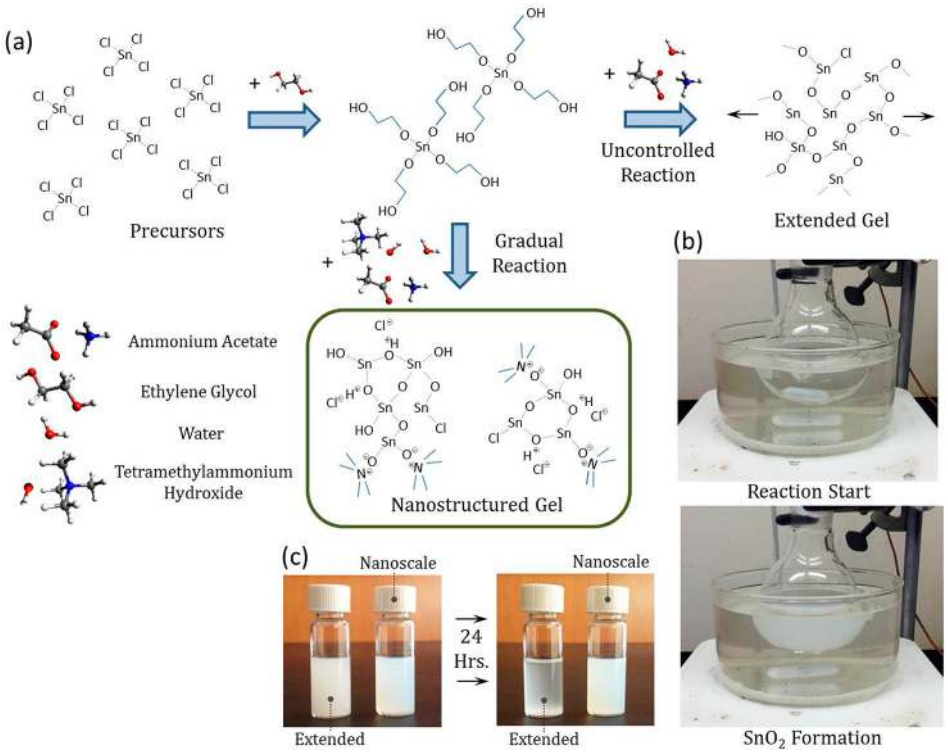

Figure 1. (a) Schematic diagram of the proposed reaction mechanism. Nanoscale dispersions are formed when tetramethylammonium is included in the reaction mixture, most likely acting as a ligand to separate the growing nanoparticles. The compounds formed by mixing $SnCl_4$ and ethylene glycol are expected to have a mixture of −Cl and $-(CH_2CH_2OH)$ groups, with the structures shown at stage 2 of the reaction depicted as fully alcoholyzed for clarity. (b) Images of the reaction mixture immediately after the addition of the reagents and after the formation of the tin oxide nanoparticles is nearly completed. (c) Images of the nanostructured and extended particle dispersions immediately after agitation and after 24 h of settling time.

RESULTS AND DISCUSSION

After several minutes of reaction time, the mixture begins showing a hazy iridescence that indicates the onset of nanoparticle formation. The reaction speed appears to be controlled most strongly by the reaction pH, and by the concentration of water in the final reaction solution, with higher pH values and higher water concentrations causing the reaction to proceed substantially faster. The balance between the rapid hydrolysis of metal species in aqueous solutions and the relatively slow kinetics of the somewhat viscous ethylene glycol precursor system ultimately allows for the controlled synthesis of well-dispersed nanoscale tin oxide particles over a period of 1−2 h.

A schematic representation of the reaction process is shown in Figure 1. The growing nanoparticles form slowly, first as a barely visible haze that ultimately produces a gray cloudy mixture. Appropriate management of the reaction sequence is necessary in order to produce highly dispersible morphologies among the resulting nanoparticles, as exhibited by the rapid settling of the products of reactions run without alkylammonium to separate the growing gel particles, as shown in the settling images in Figure 1c. Upon washing with ethanol and centrifuging, the agglomerated nanoparticles occupy a large volume of 10−20 cm^3/g SnO_2, offering evidence of the gel-like nature of the nanostructured products. Larger particles obtained from reactions run without sufficiently coordinating ligands settled to a final volume of well under 1 cm^3 per gram, comparable to the density expected from bulk SnO_2.

The structural properties of the nanoparticle films as determined by X-ray diffraction (XRD) and Raman spectroscopy are shown in Figure 2. After only a gentle annealing at 100 °C, the crystal structure clearly follows that of rutile SnO_2 (cassiterite), with broad peaks appropriate to the small size of the individual crystallites. The film crystallizes further at temperatures above 400 °C, as shown in the high-temperature spectrum at the top of Figure 2a. The approximate grain size as determined by the fwhm of the (110) peak is 2.1 nm at 100 °C and 6.8 nm at 500 °C, indicating the presence of significant but not dramatic ripening within the film.

The Raman spectra shown in Figure 2b provide some insight into the species still present in the nanoparticle dispersion after the conversion to SnO_2 is completed. In the sample annealed at 100 °C, the main Raman peak of $SnCl_4 \cdot 5H_2O$ is visible, although it is substantially weaker than that of pure tin(IV) chloride. The almost-complete removal of the tin chloride peak after high-temperature annealing suggests that the excess chloride may be located primarily on the tin oxide surface, but the small particle size of the nanostructured gels does allow for the possibility of excess chloride diffusing out from the center of a given crystallite before volatilizing out of the sample. Small peaks associated with ammonium acetate and tetramethylammonium salts can be removed by several additional washing cycles in water or ethanol, indicating that these species exist as ligands on the particle surface, and are not incorporated into the particles themselves.

The crystalline tin oxide peak, visible at ∼635 cm^{-1}, is present in Figure 2b in both the 100 °C and 500 °C tin oxide samples, but becomes sharper and much more intense at the higher annealing temperature. The broad Raman signal occurring over the range of 400−700 cm^{-1} appears to originate

dx.doi.org/10.1021/cm402462m | Chem. Mater. XXXX, XXX, XXX−XXX

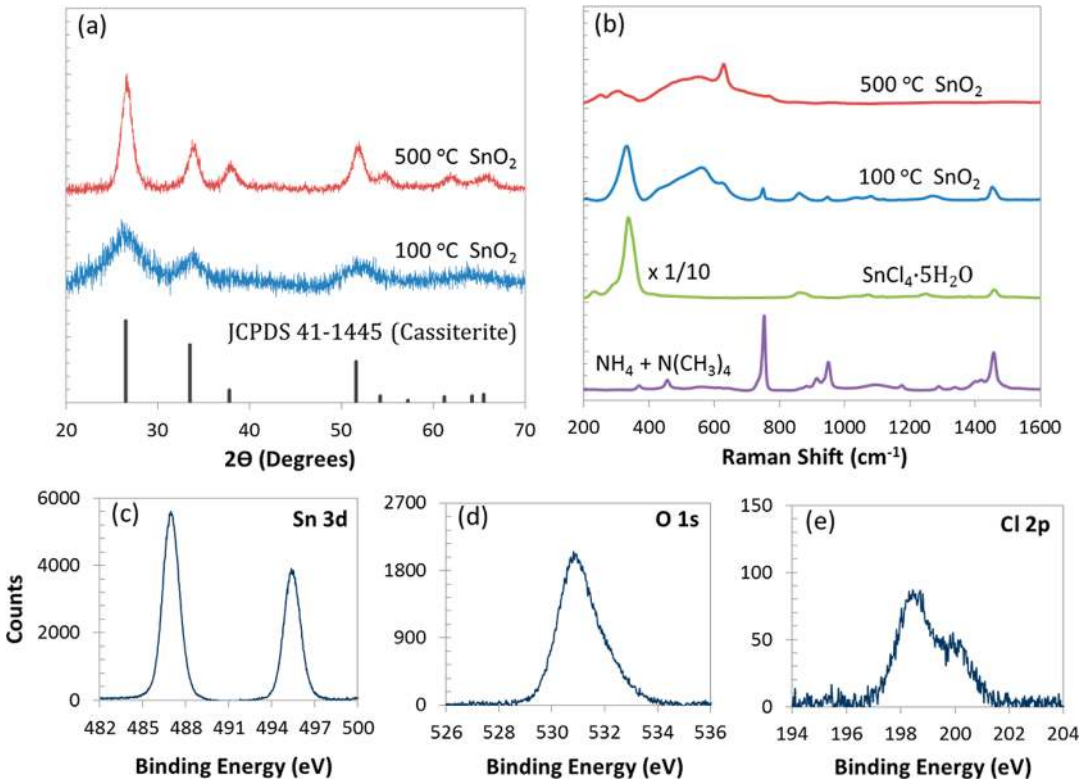

Figure 2. (a) X-ray diffraction (XRD) spectra of nanoscale SnO_2 dispersions after a gentle heat treatment at 100 °C and after a high-temperature annealing step at 500 °C, each for 15 min. The cassiterite SnO_2 phase is visible in both spectra, with appropriate peak widths for particle sizes of 2.1 and 6.8 nm. (b) Raman spectra of nanoscale SnO_2 dispersions after heat treatments at 100 and 500 °C. Also shown are Raman spectra of dried films of expected impurity and ligand materials, which are present in small quantities in the low-temperature SnO_2 sample and almost completely removed in the high-temperature SnO_2 sample. (c–e) X-ray photoelectron spectroscopy (XPS) spectra showing the Sn peaks (panel c), O peak (panel d), and Cl peaks (panel e) of a low-temperature SnO_2 sample.

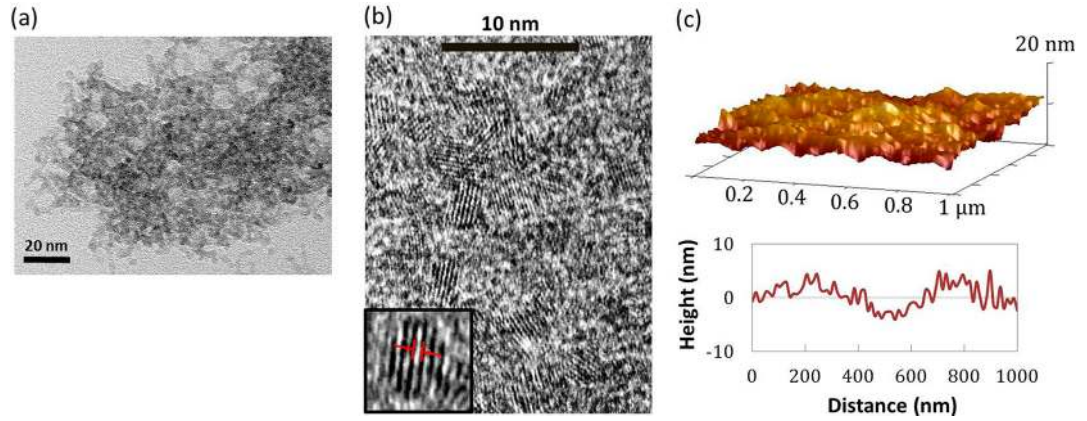

Figure 3. (a) Low-magnification and (b) high-magnification TEM images of the as-synthesized SnO_2 nanoparticles, showing typical diameters between 2 nm and 4 nm. The inset shows a close-up of one particle with the (110) lattice spacing of rutile SnO_2 (~3.35 Å) marked in red. (c) Atomic force microscopy (AFM) image of a nanoscale tin oxide film spin coated onto an oxidized silicon substrate. A representative cross section is shown below the image, showing small roughness features on the scale of individual nanoparticles and long-range features as the film thickness changes gradually across the sample surface.

from the various tin oxide bonding structures present in the gelled tin oxide films, with the disordered nature of the material readily discernible from its broad shape, even after a high-temperature annealing step. Additional analysis will be required in order to determine how much information about the local bonding environment of the individual atoms can be extracted from the shape and intensity of this particular signal.

X-ray photoelectron spectroscopy (XPS) measurements were conducted to assist with determining the state of the reaction, and the extent of conversion between $SnCl_4$ and SnO_2. The elemental signal from tin, oxygen, and chlorine is shown in Figure 2c. Integrating the peaks and correcting for XPS sensitivity and emission efficiencies allows us to determine the quantity of remaining chloride in the sample to be approximately $[Cl]/[O + Cl] \approx 3.85$ at. %, indicating that more than 96% of the anions in the material have been successfully converted to oxygen. The shoulder on the high-energy side of the O peak could arise from several sources;

dx.doi.org/10.1021/cm402462m | Chem. Mater. XXXX, XXX, XXX–XXX

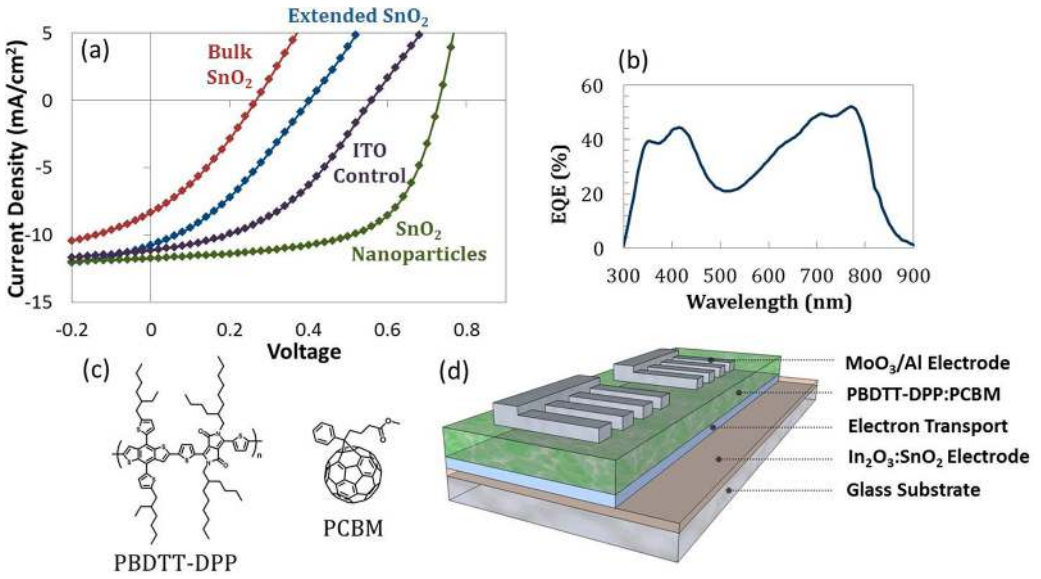

Figure 4. (a) Current−voltage (I−V) characteristics of PBDTT-DPP:PCBM solar cells using nanoscale SnO_2 as an electron transport layer (ETL), along with several control devices. The bulk SnO_2 was formed by annealing the SnO_2 nanoparticles at 450 °C, while the extended SnO_2 device used poorly formed dispersions of SnO_2, as depicted in Figure 1. (b) External quantum efficiency (EQE) data from a nanoscale SnO_2 ETL device. (c, d) Schematic diagrams of the active materials and device architecture used in solar cell fabrication. The cell is illuminated through the glass superstrate during current density−voltage (J−V) measurements.

however, at this time, we believe that it may be a result of the hydroxyl groups present throughout the gelled network of particles. The presence of small but observable numbers of Cl^- ions, along with a potentially significant number of terminating −OH groups in the sample, can both serve as markers of the small particle size and large capacity for surface ligands, and also of the relatively porous nature of the metal oxide network within the tin oxide phase. Further densification through thermal annealing, photoactivation, or other methods would likely reduce the intensity of both of these signals.

Nanoparticle morphology was determined for isolated nanoparticles using bright-field TEM imaging, and is shown in Figure 3a. The nanoparticles are extremely small, and nearly all of them have diameters between 2 nm and 4 nm. They exhibit a tendency to cluster together upon deposition, possibly due to small amounts of cross-linking and shared bonds between particles. The general propensity for aggregation among the nanoparticles does not appear to present barriers to film deposition, and instead facilitates the formation of dense, compact films that contain no detectable voids or inhomogeneous surface features.

Figure 3b shows contact-mode AFM data from a spin-coated nanoparticle film. The ∼15-nm-thick films show a root-mean-square (rms) roughness of ∼2.2 nm, which corresponds to surface oscillations on the order of a single nanoparticle diameter. The gelled nanoparticles are small enough that it is nearly impossible to distinguish individual particles, and their small size is clearly beneficial in producing smooth and continuous films. Despite the almost nonexistence of voids within these films, some care must be taken during deposition in order to ensure that the films are able to fully wet the substrate, and a UV/ozone or similar pretreatment is necessary in order to attain appropriate surface coverage when depositing onto hydrophobic materials.

Organic photovoltaic devices based on a polymer:fullerene heterojunction were fabricated in order to demonstrate the electronic properties of the tin oxide films. As an n-type semiconductor, tin oxide films have been reported as a selective contact to extract electrons from the heterojunction while rejecting holes.[23] SnO_2 represents a somewhat unique case among electron transport materials, because of the relatively low position of its conduction band. It has been reported to benefit from the presence of a small number of nonhydrolyzed bonds and oxygen vacancies, which have the combined effect of increasing the material's conductivity and reducing the relatively high work function of the bulk material.[24] The solution process employed here, with its partially incomplete conversion of alcoholyzed tin chloride to tin oxide, can be expected to capitalize on an effective reduction in work function due to the presence of high-energy bonding structures that were not completely converted to the oxide phase during the synthesis reaction. As most of the metal-oxide bonds are formed prior to film deposition, relatively little heat treatment is required to convert the material into a form that is useful for integration into devices. This allows the film to be either deposited on the substrate or possibly on top of the active layer without risking unnecessary damage to the polymer materials.

Solar cells were fabricated following the device structure shown Figure 4. Blends of the polymer PBDTT-DPP and PCBM were used as the absorber layer in this cell structure,[25] with an SnO_2/ITO front electrode providing a selective contact for collecting photogenerated electrons and an MoO_3/Al back contact for collecting holes. Data from devices using a bare ITO cathode and two alternative tin oxide suspensions are provided for comparison, with the extended SnO_2 curve resulting from the use of a poorly controlled gel reaction to synthesize the SnO_2 used as the electron transport layer. The bulk SnO_2 data uses an electron transport layer formed by annealing a nanocrystalline SnO_2 film at 450 °C for 10 min, which brings its structural properties much closer to those of the bulk material.

The different device structures exhibit a substantial variation in open circuit voltage, as shown in Table 1, with the nanoscale tin oxide devices providing markedly improved performance

dx.doi.org/10.1021/cm402462m | Chem. Mater. XXXX, XXX, XXX−XXX

Table 1. Photovoltaic Parameters of Solar Cells Made Using Different Electron Transport Layer Recipes

device structure	open-circuit voltage, V_{OC} (V)	short-circuit current density, J_{sc} (mA/cm^2)	fill factor, FF (%)	power conversion efficiency, PCE (%)
nanoscale SnO_2	0.73	11.74	61.2	5.24
bare ITO	0.56	11.15	42.9	2.67
extended SnO_2	0.40	10.78	33.6	1.45
bulk SnO_2	0.27	8.35	31.7	0.70

over the others. We expect that the presence of relatively large particles in the extended SnO_2 suspension prevented the formation of the thin, smooth, electron transport layers that are necessary for the fabrication of high-efficiency devices. The presence of shunting pathways and local disruptions in active layer morphology would then be responsible for the reduction in open-circuit voltage (V_{OC}) of this device structure, which typically produces V_{OC} values even lower than that of bare indium tin oxide (ITO) devices. The dramatic improvement in both voltage and fill factor (FF) of the nanostructured gel over its bulk counterpart suggests that the two materials are electronically distinct from each other, and provides evidence for the advantages of the nanocrystalline nature and incomplete hydrolysis that can be present in solvothermal sol−gel synthesis reactions. A more detailed investigation of the electronic properties of the two materials will be necessary in order to define the origin and the extent of their differences accurately.

The small particle size, smooth film morphology, and favorable electronic properties of the nanoscale tin oxide transport layers appear to provide an effective foundation upon which to grow polymer active layers. Future studies of the precise structure of the polymer:fullerene films may offer additional insight into whether or not significant changes are induced in the morphology of the active layer as a result of the precise surface structure of the SnO_2/ITO electrode.

CONCLUSION

We have developed a solvothermal route for the fabrication of nanocrystalline tin(IV) oxide dispersions at reaction temperatures ∼150 °C. Particles synthesized using this procedure show excellent dispersibility in polar solvents, and average particle diameters of 2−4 nm. The use of stabilized tin precursors and tetramethylammonium complexing agents during the synthesis reactions allows for the formation of products that exhibit the desirable morphological properties for use in the formation of smooth, continuous films. Tin oxide films produced using this recipe have been used as an electron transport layer in organic photovoltaic cells with conversion efficiencies above 5% under AM1.5G testing conditions. Given the large number of applications currently available to nanostructured oxides and related materials, we expect that similarly synthesized particles will find uses in a variety of optoelectronic applications that require low-temperature deposition procedures, including batteries, logic circuits, and transparent electronics.

EXPERIMENTAL METHODS

Nanoparticle Synthesis. Tin chloride pentahydrate ($SnCl_4 \cdot 5H_2O$) was dissolved in ethylene glycol by stirring for several hours at a concentration of 10 g per 80 mL to serve as a stock solution. In a typical synthesis reaction, 10 mL of $SnCl_4 \cdot 5H_2O$ stock solution and 10 mL of ethylene glycol were added to a 100-mL flask and stirred at room temperature. Still at room temperature, 2 mL of acetic acid (glacial), 1 mL of tetramethylammonium hydroxide (10% in water), and 1 mL of ammonium hydroxide (30% solution in H_2O) were added to regulate the solution pH and provide a source of water for the hydrolysis reaction. *[Note: Use caution when handling tetramethylammonium hydroxide.]* The resulting solution was immersed in an oil bath at 150 °C for at least 2 h. If the reaction occurs too quickly, the amount of 30% NH_4OH solution can be reduced to limit both the pH value and the amount of water present. Some yellowing of the solvent is commonly observed as the reaction progresses.

After the reaction was completed and cooled to room temperature, the mixture was diluted in ethanol to a total volume of 40 mL and centrifuged at 2500 rpm for 20 min. The supernatant was discarded, and the resulting solids were dispersed in ethanol by ultrasonication. The resulting dispersion in ethanol was centrifuged two more times at 2000 rpm for 20 min, and the product was dispersed again in ethanol at a concentration of 20 mg/mL. Synthetic yields typically reached values of ∼75% by weight after the completion of the washing and purification steps. This solution was used to form films and powders for structural and electronic characterization, and was diluted 2−4 times for solar cell fabrication. Extended SnO_2 gels were synthesized without any tetramethylammonium salts, with products synthesized in this manner generally showing significantly larger batch-to-batch variation than the nanoscale synthesis recipe.

Material Characterization. Samples for X-ray diffraction (XRD) and Raman analysis were prepared by drop casting the tin oxide solution onto glass slides and heating to the desired temperature. For Raman characterization, the dried tin oxide was scratched off the glass slide and onto a sputtered molybdenum film in order to reduce the amount of signal arising from the substrate. XRD and Raman characterization was performed using a PANanalytical X'Pert pro X-ray diffractometer using Cu Kα radiation ($\lambda \approx 1.54$ Å) and a Renishaw inVia confocal Raman system in a backscattering configuration. TEM samples were produced by drop-casting diluted SnO_2 solutions onto a copper TEM grid, and imaged using an FEI Titan 80−300 kV S/TEM system. Atomic force microscopy (AFM) and X-ray photoelectron spectroscopy (XPS) samples were made by spin coating thin films onto SiO_2 substrates, and these samples were measured using a Veeco Dimension 5000 scanning probe microscope and an Omicron XPS/UPS system, respectively.

Photovoltaic Device Fabrication. ITO-coated glass slides cleaned with detergent, acetone, and isopropyl alcohol were used as substrates for solar cell fabrication. The substrates were first treated with an ultraviolet lamp in the presence of oxygen for 15 min in order to adjust their surface properties. In SnO_2 devices, tin oxide films were then deposited by spin coating at 5000 rpm, and then heating at 150 °C for 10 min. Instead, bulk SnO_2 samples were heated to 450 °C for 10 min. The PBDTT-DPP absorber layers were deposited by spin-casting a 1:2 PBDTT-DPP:PC_{60}BM blend (by weight) with a total solution concentration of 0.7 wt % in dichlorobenzene. MoO_3/Al electrodes were then deposited by thermal evaporation in high vacuum to complete the devices. Photovoltaic measurements were carried out using a Newport Oriel solar simulator under 100 mW/cm^2 illumination verified immediately prior to measurement using a calibrated photodiode. External quantum efficiency (EQE) measurements were made using an EQE system from Enlitech.

AUTHOR INFORMATION

Corresponding Author

*Tel.: 310-825-4052. Fax: 310-825-3665. E-mail: yangy@ucla.edu.

Notes

The authors declare no competing financial interest.

ACKNOWLEDGMENTS

This work was supported in part by NSF Grant No. ECCS 1202231. The authors would like to acknowledge the use of the

Electron Imaging Center for Nanomachines (EICN) and the Nano-Pico Characterization Lab (NPCL), both located in the California NanoSystems Institute at UCLA.

REFERENCES

(1) Dattoli, E. N.; Wan, Q.; Guo, W.; Chen, Y.; Pan, X.; Lu, W. *Nano Lett.* **2007**, *7*, 2463−2469.
(2) Presley, R. E.; Munsee, C. L.; Park, C.-H.; Hong, D.; Wager, J. F.; Keszler, D. A. *J. Phys. D* **2004**, *37*, 2810−2813.
(3) Sun, J.; Lu, A.; Wang, L.; Hu, Y.; Wan, Q. *Nanotechnology* **2009**, *20*, 335204.
(4) Snaith, H.; Ducati, C. *Nano Lett.* **2010**, *10*, 1259−1265.
(5) Hossain, M.; Jennings, J.; Koh, Z.; Wang, Q. *ACS Nano* **2011**, *5*, 3172−3181.
(6) Chopra, L.; Paulson, P. D.; Dutta, V.; K.. *Prog. Photovolt.: Res. Appl.* **2004**, *12*, 69−92.
(7) Qian, J.; Liu, P.; Xiao, Y.; Jiang, Y.; Cao, Y. *Adv. Mater.* **2009**, *21*, 3663−3667.
(8) Kim, C.; Noh, M.; Choi, M.; Cho, J.; Park, B. *Chem. Mater.* **2005**, 3297−3301.
(9) Meduri, P.; Pendyala, C.; Kumar, V.; Sumanasekera, G. U.; Sunkara, M. K. *Nano Lett.* **2009**, *9*, 612−616.
(10) Idota, Y. *Science* **1997**, *276*, 1395−1397.
(11) Kida, T.; Doi, T.; Shimanoe, K. *Chem. Mater.* **2010**, *22*, 2662−2667.
(12) Lin, R.; Luo, M.; Zhong, Y.; Yan, Z. *Appl. Catal., A* **2003**, *255*, 331−336.
(13) Vinodgopal, K.; Bedja, I.; Kamat, P. *Chem. Mater.* **1996**, *8*, 2180−2187.
(14) Gyger, F.; Hubner, M.; Feldmann, C. *Chem. Mater.* **2010**, *22*, 4821−4827.
(15) Jang, J.; Kitsomboonloha, R.; Swisher, S. L.; Park, E. S.; Kang, H.; Subramanian, V. *Adv. Mater.* **2013**, *25*, 1042−1047.
(16) Yella, A.; Lee, H.-W.; Tsao, H. N.; Yi, C.; Chandiran, A. K.; Nazeeruddin, M. K.; Diau, E. W.-G.; Yeh, C.-Y.; Zakeeruddin, S. M.; Grätzel, M. *Science* **2011**, *334*, 629−634.
(17) Ito, S.; Murakami, T. N.; Comte, P.; Liska, P.; Grätzel, C.; Nazeeruddin, M. K.; Grätzel, M. *Thin Solid Films* **2008**, *516*, 4613−4619.
(18) Rech, B.; Wagner, H. *Appl. Phys. A: Mater. Sci. Process.* **1999**, *69*, 155−167.
(19) Britt, J.; Ferekides, C. *Appl. Phys. Lett.* **1993**, *62*, 2851−2852.
(20) Larramona, G.; Choné, C.; Jacob, A. *Chem. Mater.* **2006**, *18*, 1688−1696.
(21) Zhuang, Z.; Huang, F.; Lin, Z.; Zhang, H. *J. Am. Chem. Soc.* **2012**, *134*, 16228−16234.
(22) Yu, C.; Yu, J. C.; Wang, F.; Wen, H.; Tang, Y. *Cryst. Eng. Commun.* **2010**, *12*, 341.
(23) Lee, Y.-I.; Youn, J.-H.; Ryu, M.-S.; Kim, J.; Moon, H.-T.; Jang, J. *Curr. Appl. Phys.* **2012**, *12*, 46−48.
(24) Trost, S.; Zilberberg, K.; Behrendt, A.; Riedl, T. *J. Mater. Chem.* **2012**, *22*, 16224.
(25) Dou, L.; Gao, J.; Richard, E.; You, J.; Chen, C.-C.; Cha, K. C.; He, Y.; Yang, Y. *J. Am. Chem. Soc.* **2012**, *134*, 10071−10079.